72-9038

KAYE, George Edwin, 1941-
FEASIBILITY OF X-RAY FLUORESCENCE FOR IN VIVO DIAGNOSIS OF MERCURY.

The University of Oklahoma, Ph.D., 1971
Health Sciences, radiology

University Microfilms, A XEROX Company, Ann Arbor, Michigan

THIS DISSERTATION HAS BEEN MICROFILMED EXACTLY AS RECEIVED

THE UNIVERSITY OF OKLAHOMA

GRADUATE COLLEGE

FEASIBILITY OF X-RAY FLUORESCENCE FOR IN VIVO DIAGNOSIS OF MERCURY

A DISSERTATION

SUBMITTED TO THE GRADUATE FACULTY

in partial fulfillment of the requirements for the degree of

DOCTOR OF PHILOSOPHY

BY

GEORGE EDWIN KAYE

Norman, Oklahoma

1971

FEASIBILITY OF X-RAY FLUORESCENCE FOR

IN VIVO DIAGNOSIS OF MERCURY

APPROVED BY

Robert J. Nelson

Larry Canter

James M. Robertson

Winfield W. Evans

C. N. Lawrence

DISSERTATION COMMITTEE

PLEASE NOTE:

Some Pages have indistinct print. Filmed as received.

UNIVERSITY MICROFILMS

ACKNOWLEDGMENTS

This writer acknowledges Jesus Christ to be the Son of the true and living God and the Holy Spirit to be the Comforter of those in need.

He further acknowledges the following people and organizations without whose help this dissertation could not have been completed:

Robert Y. Nelson for the opportunity to do graduate work and for his advice and technical assistance in directing this work.

Winfield W. Evans for his many hours of discussion and help in preparing this dissertation.

The entire committee for their advice and help in preparing this dissertation.

United States Public Health Service for their support in the form of a Training Grant.

My children for their interest.

And my wife Mary Jane for typing this into manuscript form and for her love, help and encouragement.

TABLE OF CONTENTS

LIST OF TABLES

LIST OF ILLUSTRATIONS

LIST OF ILLUSTRATIONS - Continued

NOMENCLATURE

$d({}_e\sigma)$	=	Klein-Nishina collision differential cross section
E_L	=	energy of the L fluorescent line
E_n	=	energy of the n shell absorption edge
E_o	=	energy of the incident photon
E'	=	energy of the Compton scattered photon
r_n	=	n shell absorption jump ratio
ω_K	=	K shell fluorescent yield
ω_L	=	L shell fluorescent yield
Φ	=	photon fluence in photons/cm^2
φ	=	photon flux density in photons/cm^2-sec
Φ_{gen}	=	X-ray tube generated photon fluence
Φ_{in,E_o}	=	monoenergetic incident photon fluence
$\Phi_{in}(E_o)$	=	energy distribution of incident photon fluence
$\Delta\Phi_D$	=	total partial fluence at detector
$\Delta\Phi_{D,E_L}$	=	partial fluence at detector from line E_L
$\Delta\Phi_{D,C,E'}$	=	partial fluence at detector due to Compton scatter of a monoenergetic photon
$\Delta\Phi_{D,C}(E')$	=	partial fluence at detector due to Compton scatter from an energy distribution of photons

Additional symbols are defined at the point of their use.

FEASIBILITY OF X-RAY FLUORESCENCE FOR IN VIVO DIAGNOSIS OF MERCURY

CHAPTER I

INTRODUCTION

General

The process of resonance fluorescence has come under investigation for its prospective uses in diagnostic nuclear medicine. This investigation has been directed at both improving current procedures and developing new procedures that are not possible by other methods.

One of the more useful procedures in nuclear medicine is organ scanning. This is classically performed by first, administering a radiopharmaceutical that will undergo uptake by the particular organ in question and second, counting the photons emitted by the radioisotope. Although much progress has been made in the development of suitable pharmaceuticals and sophisticated instrumentation, there still remain several disadvantages inherent in the process including residual radiation dose from the radioisotope (effective half-life), beta particle dose, and irradiation of other parts of the body.

Organ scanning by resonance fluorescence has recently been explored by Tinney (1967), Hoffer et al.

(1968), and Patton et al. (1970). This method may utilize an element that is already present in the organ, e.g. iodine in the thyroid, or if no such element exists in adequate concentration, an element that will be taken up by the organ in question may be administered. The scan is obtained by scanning simultaneously with an input X-ray or γ-ray beam and a fluorescent X-ray detector. In addition to overcoming several of the disadvantages of the radioactive isotope method, an advantage of resonance fluorescence is that it allows all of the high atomic number elements to be considered in organ scanning.

Additional investigations that have recently been reported on the applications of fluorescence include tomographic scanning and blood flow. Patton et al. (1970) have reported on using bismuth as a trace metal in brain scanning. Hoffer et al. (1969b) have extended their investigations into a determination of cerebral blood flow using iodine. These examples suggest only a starting point for the usefulness of resonance fluorescence in nuclear medicine.

Objective

The principal element studied thus far as a trace element in fluorescence has been iodine. The fact that iodine is natural occurring in the body in relatively high concentration is perhaps the most important reason for its popularity thus far. Bismuth has been investigated because of its high preferential uptake by diseased brain

tissue. The toxicity of bismuth is such that extremely sensitive detection methods must be used in order to keep the body concentrations low.

In exploring the usefulness of the very heavy metals, several factors are of importance. The physical property of the high atomic number elements that makes them more useful in the fluorescence process is the high K and L shell energies and consequently high fluorescent photon energies. As the atomic number increases; however, the energy required to excite a given atomic shell increases. Most investigators have used the relatively abundant radionuclide, Americium-241, as their excitation source. The 60 keV gamma ray given off by this radionuclide effectively excites K-shell fluorescence in those elements whose K shell absorption edge is below 60 keV. This property limits the usefulness of this radionuclide drastically when the atomic number of the trace element is increased beyond 69 (Thulium). For this reason another source of excitation must be used in studying elements with atomic numbers larger than 69.

This investigation is designed to determine the feasibility of extending the technique of resonance fluorescence to the high atomic number elements. The element mercury (atomic number 80) was chosen for this investigation because it is abundant in nature and its physiological behavior and toxicology are well known. Since X-ray generators are readily available and they would

make an economical source of excitation for use in diagnostic procedures, an X-ray generator was chosen for this investigation. The results from the experiment could then be used to predict the results that would be obtained if a radioisotope source had been used.

Discussion

X-ray Fluorescence

X-ray fluorescence, a special case of the more general process fluorescence, involves the excitation of the atom in the K or L electron shells. The atom subsequently emits the excess energy as it returns to the ground state. All but the lightest elements may emit this energy as a fluorescent X-ray photon with an energy characteristic of the emitting element. A second emission process competitive with fluorescence is known as the Auger effect. In this emission the atom returns to the ground state by ejecting an electron from the next higher electron shell. No photon emission occurs in this case.

The K fluorescent yield, ω_K, is defined as the number of photons of all lines in the K series emitted in unit time divided by the number of K shell vacancies formed during the same time. The L fluorescent yield, ω_L, is defined similarly for the L shell. Were it not for the Auger effect the fluorescent yield would be unity. Figure 1-1 shows the variation of fluorescent yield with atomic number and series.

If one considers the absorption coefficient to be

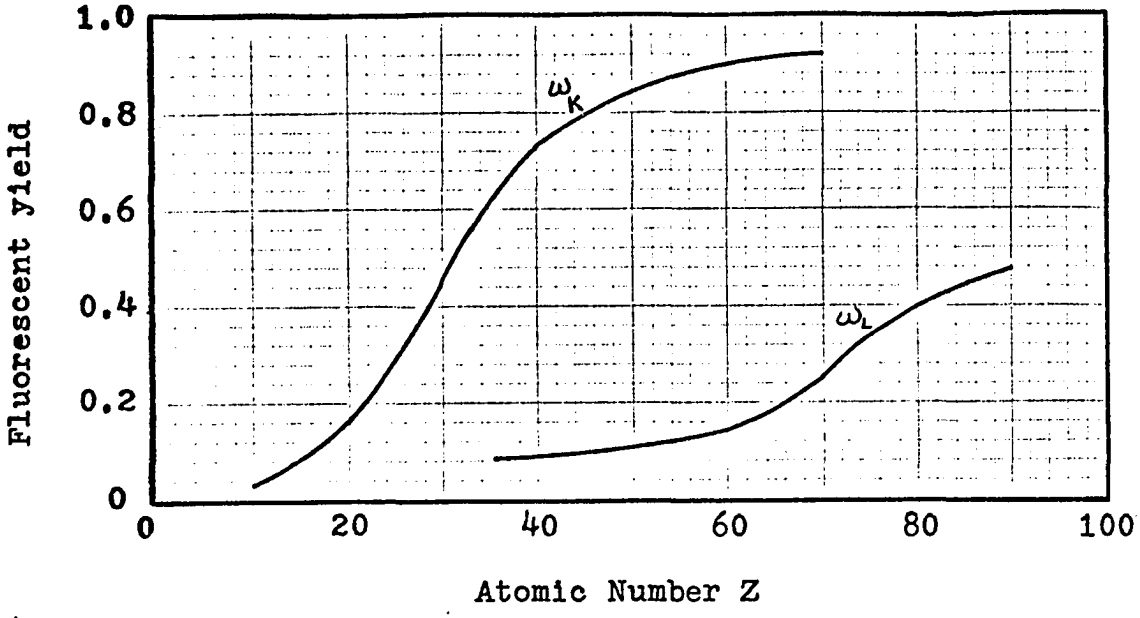

Figure 1-1. Dependence of the fluorescent yield on atomic number for the K and L electron shells (Bertin, 1970).

a discontinuous two valued function at the absorption edge energies, a ratio of the larger value to the smaller value at the discontinuity may be formed. This ratio is defined as the n shell absorption jump ratio, r_n. This factor is used to weigh the absorptions in the n^{th} shell to the absorptions in the other atomic shells for the fluorescing element.

Figure 1-2 shows the model used to derive the relationship between the incident X-ray fluence and the fluorescent X-ray fluence. The partial fluence at the detector energy E_L originating in incremental slab Δt is $\Delta\Phi_{D,E_L}$ for the L line of the n shell. Bertin (1970) has shown for monoenergetic photons of energy E_o, greater than the n shell absorption edge energy E_n, and for

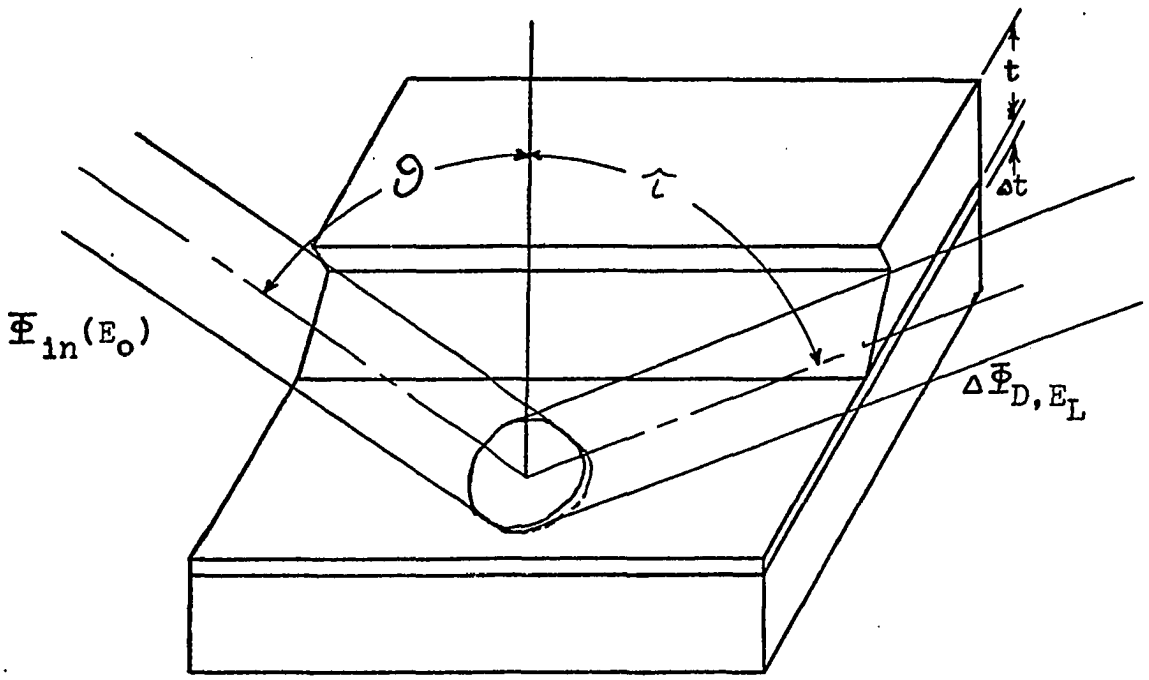

Figure 1-2. X-ray Fluorescence Model.

incidence at angle ϑ that

$$\Delta\Phi_{D,E_L} = \frac{S\Delta t \csc\vartheta}{4\pi R^2} C_A\left(\frac{r_n-1}{r_n}\right)\omega_n g_L \exp-\left\{[\mu/\rho]_{M,E_L}\rho t \csc\tau\right\}$$

$$\times [\mu/\rho]_{A,E_o} \exp-\left\{[\mu/\rho]_{M,E_o}\rho t \csc\vartheta\right\}\Phi_{in,E_o} \qquad (1\text{-}1)$$

where:

S = area of Δt exposed to beam

R = distance from Δt to detector

C_A = concentration of trace element A in gm/cm^3

r_n = n shell absorption jump ratio for trace element A

ω_n = n shell fluorescent yield for trace element A

g_L = probability of the orbital electron transition resulting in line L

$[\mu/\rho]_{M,E_o}$ and $[\mu/\rho]_{M,E_L}$ = mass attenuation coefficient of the material M at energies E_o and E_L respectively

$[\mu/\rho]_{A,E_o}$ = mass absorption coefficient of trace element A at energy E_o

and Φ_{in,E_o} = photon fluence incident on slab at energy E_o .

To consider the case where the incident photon beam is not monoenergetic, $\Phi_{in}(E_o)$ represents the distribution of fluence with respect to energy. Since only photons with energy $E > E_n$ will excite fluorescence in the n shell, $\Delta\Phi_{D,E_L}$ may be expressed as the integral

$$\Delta\Phi_{D,E_L} = \int_{E_n}^{E_{max}} f(E_o)\Phi_{in}(E_o)dE_o \qquad (1\text{-}2)$$

where $f(E_o)$ is some function of energy describing fluorescent X-ray production in the sample. By noting the energy dependent terms in equation (1-1) one may write

$$f(E_o) = \frac{S\Delta t \csc\vartheta}{4\pi R^2} C_A\left(\frac{r_n-1}{r_n}\right)\omega_n g_L \exp-\left\{[\mu/\rho]_{M,E_L}\rho t \csc\vartheta\right\}$$

$$\times [\mu/\rho]_A(E_o)\exp-\left\{[\mu/\rho]_M(E_o)\rho t \csc\vartheta\right\} . \qquad (1\text{-}3)$$

Compton Scattering

The incoherent scattering of photons by atomic electrons is known as the Compton effect. Figure 1-3

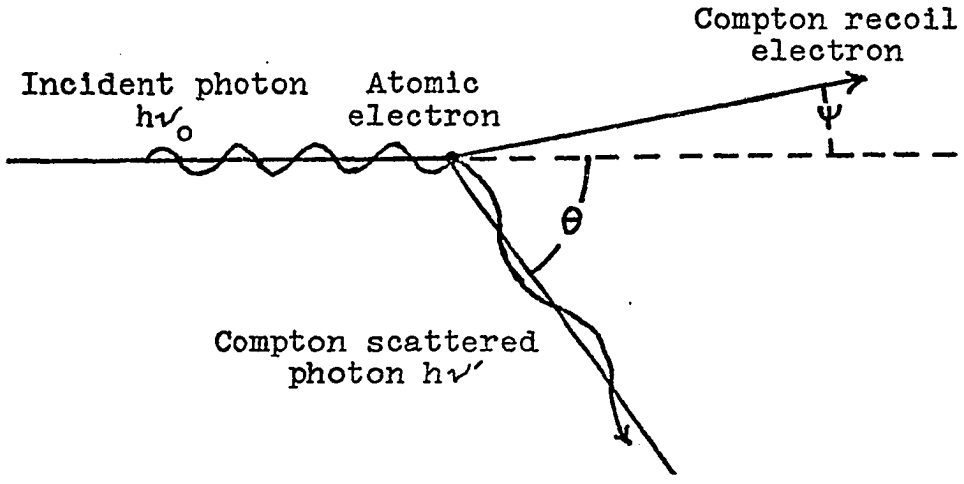

Figure 1-3. Relationship between incident photon, scattered photon, and recoil electron in the Compton scatter process.

shows the model used to relate the energies and directions of travel of the incident photon, scattered photon, and scattered electron. Compton scattering has been described in detail by Compton and Allison (1935), Evans (1955 and 1968), and Morgan and Turner (1967). The following paragraphs present the pertinent details of these discussions.

The number of photons that are Compton scattered was first formulated by Klein and Nishina (1929). The formulation known as the Klein-Nishina relation, gives the collision differential cross section as a fraction of the number of incident photons

$$d({}_e\sigma) = r_o^2 d\Omega \left[\frac{1}{1+\alpha(1-\cos\theta)}\right]^2 \left(\frac{1+\cos^2\theta}{2}\right) \times \left\{1+\frac{\alpha^2(1-\cos\theta)^2}{(1+\cos^2\theta)[1+\alpha(1-\cos\theta)]}\right\} \frac{cm^2}{electron} \qquad (1\text{-}4)$$

where:

$d({}_e\sigma)$ = collision differential cross section for unpolarized photons striking unbound, randomly oriented electrons

θ = mean scattering angle

r_o^2 = classical electron radius and has a value

$$r_o \doteq \frac{e^2}{m_o c^2} = 2.818\times10^{-13} cm$$

and α = dimensionless quantity expressing the incident photon energy as

$$\alpha \doteq \frac{h\nu_o}{m_o c^2}$$

where h_o is the incident photon energy.

The Compton shift is the difference between the energy $h\nu_o$ of the incident photon and the energy $h\nu'$ of the Compton scattered photon. The energy of the scattered photon is

$$h\nu' = \frac{m_o c^2}{1+\frac{1}{\alpha}-\cos\theta} \quad . \qquad (1\text{-}5)$$

Figure 1-4 expresses the dependence of $h\nu'$ on $h\nu_o$ for four values of the scattering angle θ.

For the case of monoenergetic incident photon fluence, the Compton scattered X-ray fluence at the detector may be evaluated by using the alternate form of equation (1-4),

$$d({}_e\sigma) = \frac{r_o^2}{2} d\Omega \left(\frac{\nu'}{\nu_o}\right)^2 \left(\frac{\nu_o}{\nu'} + \frac{\nu'}{\nu_o} - \sin^2\theta\right) \frac{cm^2}{electron} \tag{1-6}$$

where ν_o = frequency of incident photon

and ν' = frequency of scattered photon.

By using the relation $E = h\nu$ and substituting for ν_o and ν' one obtains the equation

$$d({}_e\sigma) = \frac{r_o^2}{2} d\Omega \left(\frac{E'}{E_o}\right)^2 \left(\frac{E_o}{E'} + \frac{E'}{E_o} - \sin^2\theta\right) \frac{cm^2}{electron} \tag{1-7}$$

The partial fluence at the detector due to Compton scattering is given by

$$\Delta \Phi_{D,C,E'} = \frac{r_o^2}{2} \frac{\rho_e \Delta t}{R^2} \left(\frac{E'}{E_o}\right)^2 \left(\frac{E_o}{E'} + \frac{E'}{E_o} - \sin^2\theta\right) \Phi_{in,E_o} \tag{1-8}$$

where ρ_e = electron density of scattering material

Δt = thickness of incremental slab

R = sample to detector distance

and E' = energy of scattered photon given by equation (1-5).

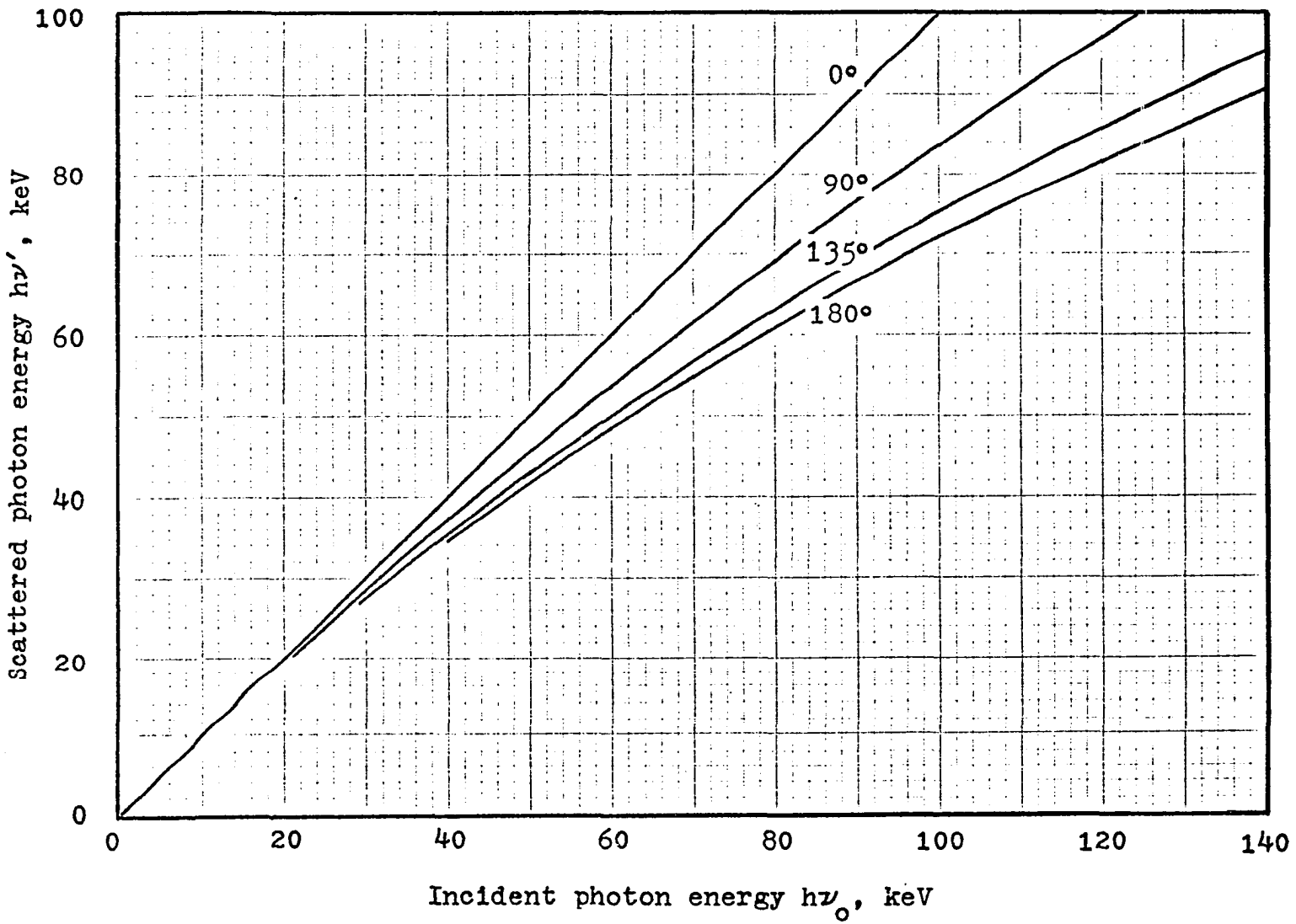

Figure 1-4. Dependence of scattered photon energy on incident photon energy and angle of scatter.

If the incident photon fluence is an energy distribution given by $\Phi_{in}(E_o)$, then the partial fluence at the detector is a distribution given by

$$\Delta\Phi_{D,C}(E') = \frac{r_o^2}{2}\frac{\rho_e \Delta t}{R^2}\left(\frac{E'}{E_o}\right)^2\left(\frac{E_o}{E'}+\frac{E'}{E_o}-\sin^2\theta\right)\Phi_{in}(E_o) \quad . \tag{1-9}$$

Detector Fluence

The photon fluence that enters the detector will consist of all the photons that are generated in the sample and enter the solid angle subtended by the detector. This photon fluence will contain X-rays from all of the fluorescent lines and the Compton scatter. From equations (1-1) and (1-8), the fluence at the detector from incremental thickness Δt is given by

$$\Delta\Phi_D = \Delta\Phi_{D,E_{L1}} + \Delta\Phi_{D,E_{L2}} + \cdots + \Delta\Phi_{D,C,E'} \tag{1-10}$$

for a monoenergetic source of excitation with energy E_o. This fluence distribution will consist of a number of discrete lines. For the case of excitation with an energy distribution of photons, equations (1-2) and (1-9) can be combined to give

$$\Delta\Phi_D = \Delta\Phi_{D,E_{L1}} + \Delta\Phi_{D,E_{L2}} + \cdots + \Delta\Phi_{D,C}(E') \quad . \tag{1-11}$$

It can be seen that the Compton contribution to the detector fluence is now a distribution of energy instead of the line contribution in equation (1-10).

X-ray Generator

The X-ray generator has several advantages over other excitation methods in X-ray fluorescence. X-ray generators are readily available, relatively inexpensive, and they are easy to control and operate. In addition they are a very high flux density source of photons. The energy distribution of fluence produced in the generator can, however, place severe limitations on the usefulness of the X-ray generator.

The energy distribution of fluence produced in the generator ranges from a few keV up to a maximum energy determined by the peak kiloVoltage applied to the tube. The only photons in this distribution function, $\Phi_{gen}(E)$, that are useful in exciting resonance fluorescence are those with energy greater than the sample n shell absorption edge. It is, therefore, reasonable to search for a more useful energy distribution of fluence.

From the discussion of excitation and from inspection of the attenuation curve shown in Figure 1-5 one sees that the incident photon energy of maximum effectiveness in exciting fluorescence is one that is at or slightly higher than the absorption edge energy.

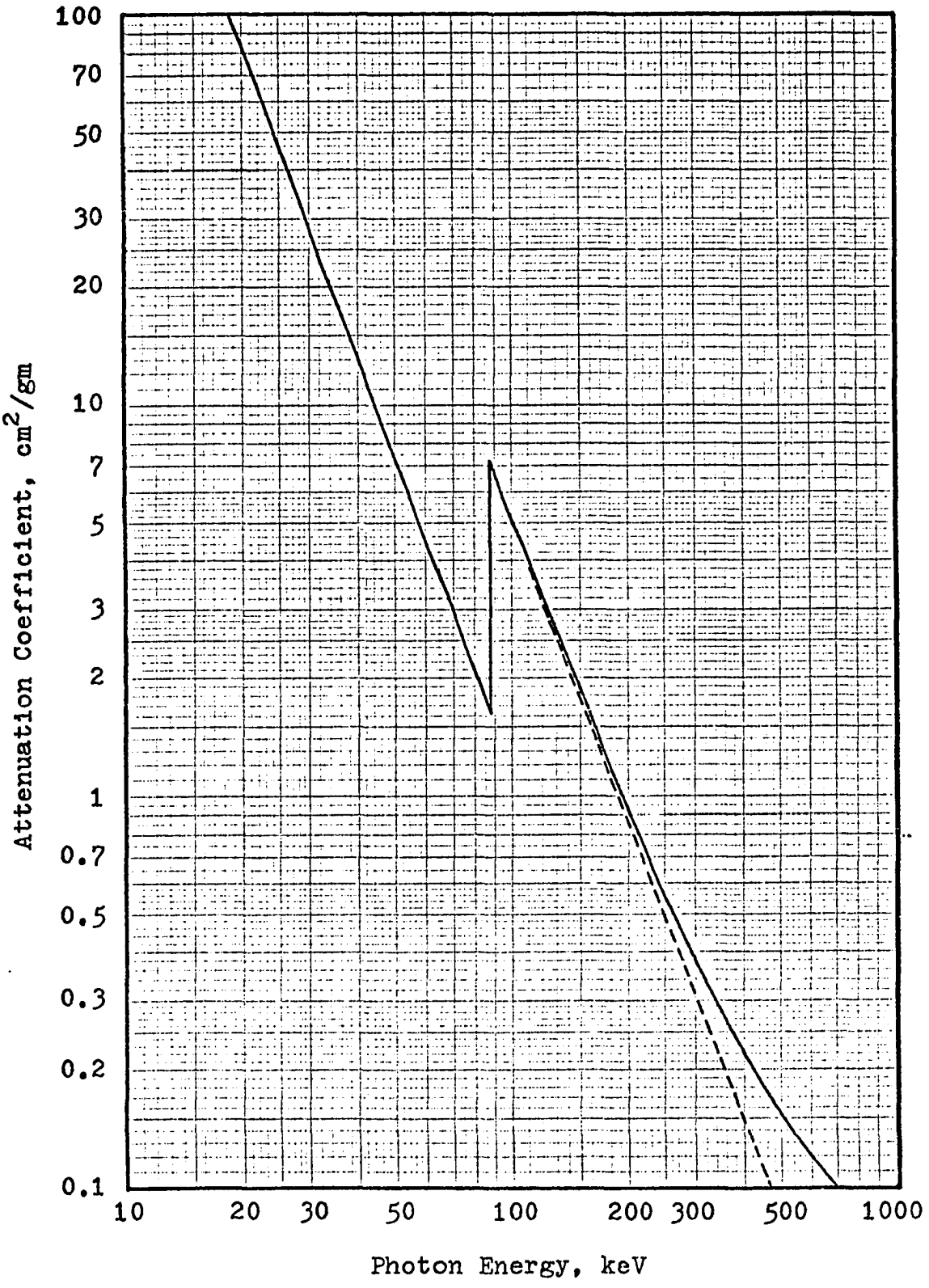

Figure 1-5. Attenuation coefficient of lead as a function of photon energy. The solid line shows total attenuation while the dashed line shows photoelectric absorption.

Therefore, $\Phi_{in}(E_o)$, the energy distribution of fluence incident on the sample, should be large above the absorption edge. Photons below this energy have a two-fold detrimental effect: they contribute significantly to the entrance dose and they create a background that may obscure the fluorescent X-ray peak.

Compton scattered X-rays entering the detector at the fluorescent X-ray energy contribute a background that is unrelated to the trace element concentration. It is necessary, therefore, that incident X-rays which will scatter to this energy be avoided. The energies of the scattered photon and the incident photon are related by equation (1-5). The restraints on $\Phi_{in}(E_o)$ are that this distribution be large immediately above the absorption edge and be sharply falling on both sides of this energy range.

The X-ray generator must include a filter that will transform the generated fluence $\Phi_{gen}(E)$ into the incident fluence $\Phi_{in}(E_o)$. One method for achieving this is with a selected thickness of high atomic number metal. Inspection of the transmission curves in Figure 1-6 will show that increasing thicknesses of filter work to create a band pass like that desired to transform $\Phi_{gen}(E)$ into $\Phi_{in}(E_o)$. This shaping is caused on the high energy side by the K-absorption edge, and on the low energy side by the steepness of the attenuation coefficient at low energy as shown in Figure 1-5.

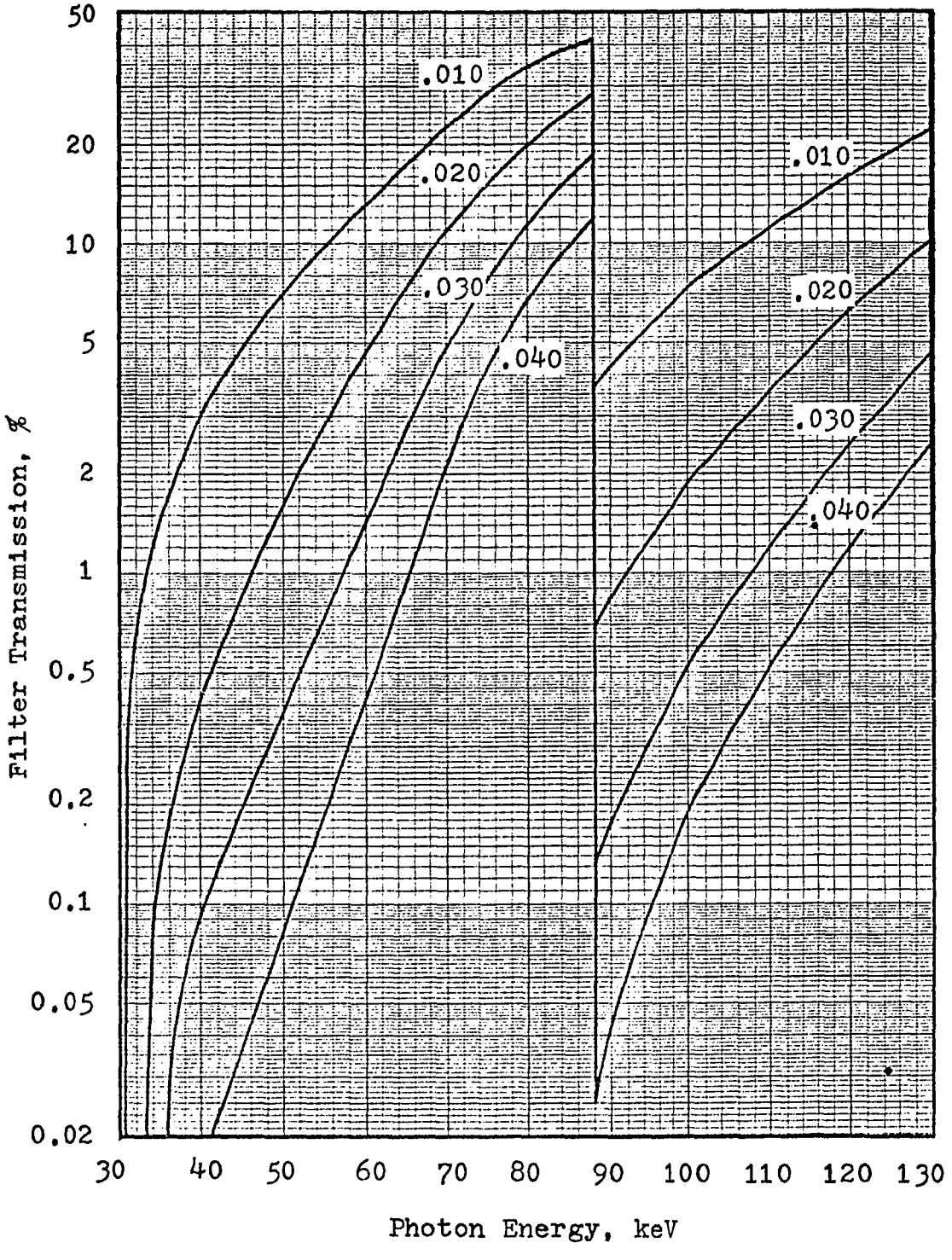

Figure 1-6. Transmission curves for increasing thicknesses of lead filter (Thicknesses measured in thousandth of an inch).

Summary

In nuclear counting the condition that gives the greatest amount of information about the sample is when the sample count is maximum and the background count is minimum. In the case of fluorescence counting with a high resolution detector this condition translates to selecting a suitable chosen energy window which contains the fluorescent line of interest. The problem then becomes one of adjusting the several variables to determine the sample count to background ratio that contains the largest amount of sample information. This may be developed further by considering the terms in equation (1-10). Each of the $\Delta\Phi_{D,E_L}$ terms contains a given amount of information about the sample; therefore, they cannot interfere with each other. On the other hand, the $\Delta\Phi_{D,C,E}$ term contains no sample information. Since the energy of this contribution is fixed by the energy of the incident fluence and the scattering angle, the energy of this Compton contribution can be adjusted so that Compton scatter poses no severe problems on the sample detectability.

For the case of excitation with an energy distribution, the $\Delta\Phi_{D,E_L}$ terms in equation (1-11) are the same as in equation (1-10). The Compton scatter term $\Delta\Phi_{D,E}(E')$ is now a distribution. This energy distribution can place a background at the energy of each fluorescent line.

This condition places a lower limit on the minimum detectable quantity of sample. This lower limit then becomes a problem of optimizing the several parameters to obtain the greatest amount of sample information from the detector fluence $\Delta\Phi_D$.

CHAPTER II

EXPERIMENTAL APPARATUS

Sample Fluorescence

X-ray Generator

The X-ray generator used in the experiment was a Westinghouse industrial radiography unit style 982036. The tube for this generator was a Thermax Industrial model B with water cooling. The generator has maximum ratings of 150 kiloVolts and 30 milliAmps; however, the cooling characteristics of the tube do not permit continuous duty at these values.

The generator control unit contains a mA stabilizer which regulates the X-ray tube filament temperature by sampling the current flowing in the X-ray tube. An increase or decrease in this current is used to adjust the filament voltage down or up respectively by means of a variable reactance in series with the filament power supply. This dynamic regulator controls the tube output to within ± 5 percent after a 2 minute warm up period.

A collimator was constructed for the X-ray tube generator by bolting a two inch floor flange to the tube housing. A one quarter inch thick slab of lead with a

one eighth inch drill hole was sandwiched between the tube housing and the floor flange. A six inch nipple of two inch iron pipe was screwed into the flange. The arrangement was such that the X-ray beam passed through the hole in the lead, through the flange, and down the axis of the iron pipe. A one quarter inch thick slab of lead was placed on the opposite end of the pipe. This slab was drilled so that a 12 mm. diameter beam was obtained at the sample. After examination of the family of curves shown in Figure 1-5, a 0.035 inch thick lead filter was chosen as the optimum value and the filter was fabricated. This filter was affixed to the target side of the second collimator. The calculated transmission curve for this filter is shown in Figure 2-1.

Beam Monitor

The exposure rate in the incident X-ray beam was monitored by means of a Victoreen model 227 ionization chamber. This chamber is cylindrical with inside diameter 28.8 mm. and length 78.0 mm. The chamber was positioned at a distance of 40 cm. from the tube target so that a beam of about one cm. in diameter was passed obliquely through the collecting volume. A charge collecting potential of 300 Volts was placed across the chamber. Because the readings were to be relative only, no attempt was made to determine absolutely the volume of the chamber exposed to the incident beam.

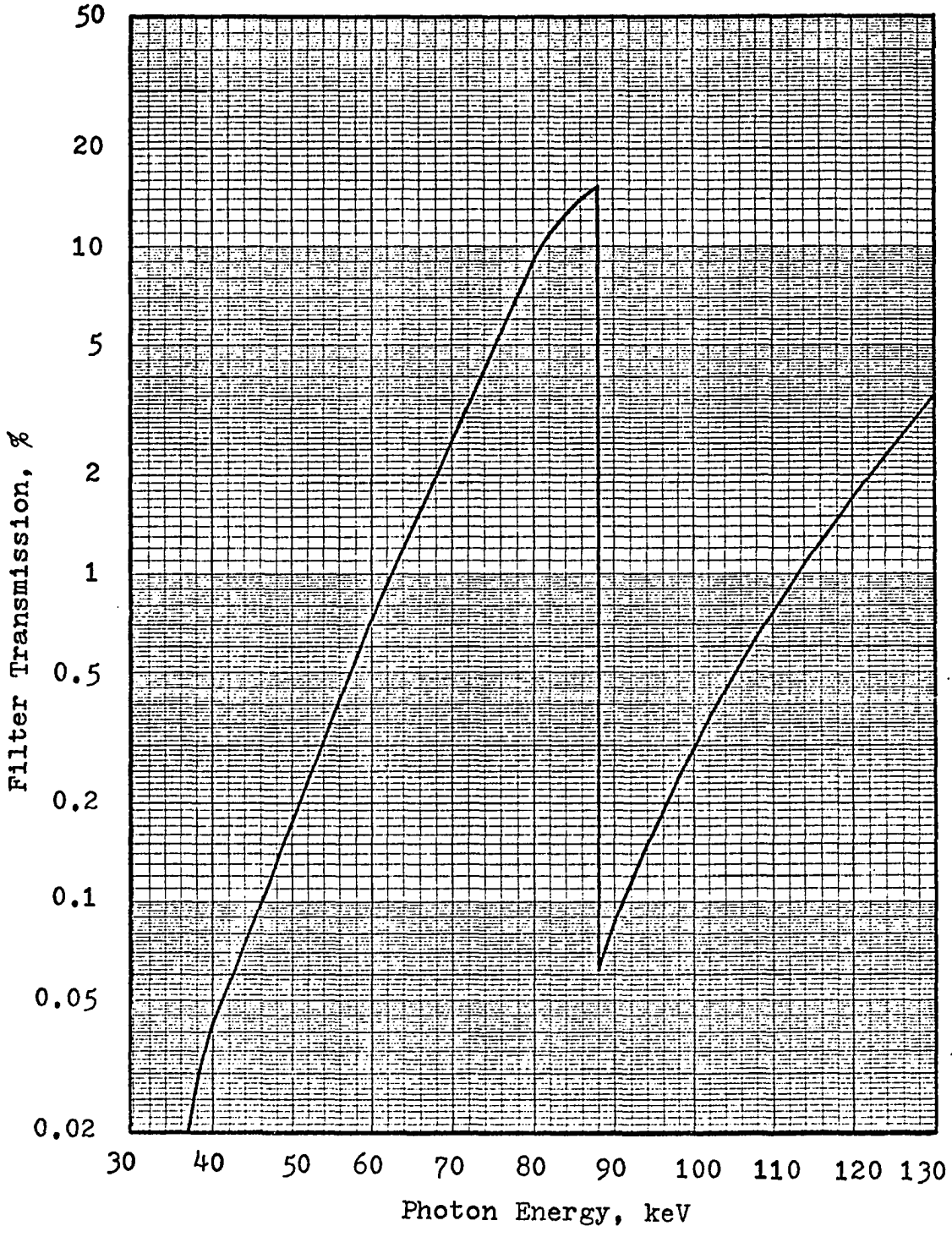

Figure 2-1. Transmission of the 0.035 inch thick lead filter.

The ionization current generated in the chamber was collected by a Cary model 31 vibrating reed electrometer. The output of the electrometer was displayed on a strip chart recorder. This readout was used to determine the integral exposure in the beam.

Sample Arrangement

The samples that were used to determine mercury concentration were prepared by diluting a stock solution of aqueous mercuric salt. The concentration of mercuric ion was determined by an independent laboratory and was reported to be 5637 ppm. Dilutions were prepared from this stock solution as shown in Table 2-1. For analysis

TABLE 2-1

SAMPLE MERCURY SOLUTION CONCENTRATIONS

Sample	Concentration ppm
Stock	5637
Dilution one	3780
Dilution two	2835
Dilution three	1890

in the experiment the solutions were placed in cylindrical polyethylene containers. These bottles had an internal diameter of 17 mm. and an internal height of 21 mm. They held a volume of 4.75 cc. For irridiation the samples were placed on a lucite stand as shown in Figure 2-2.

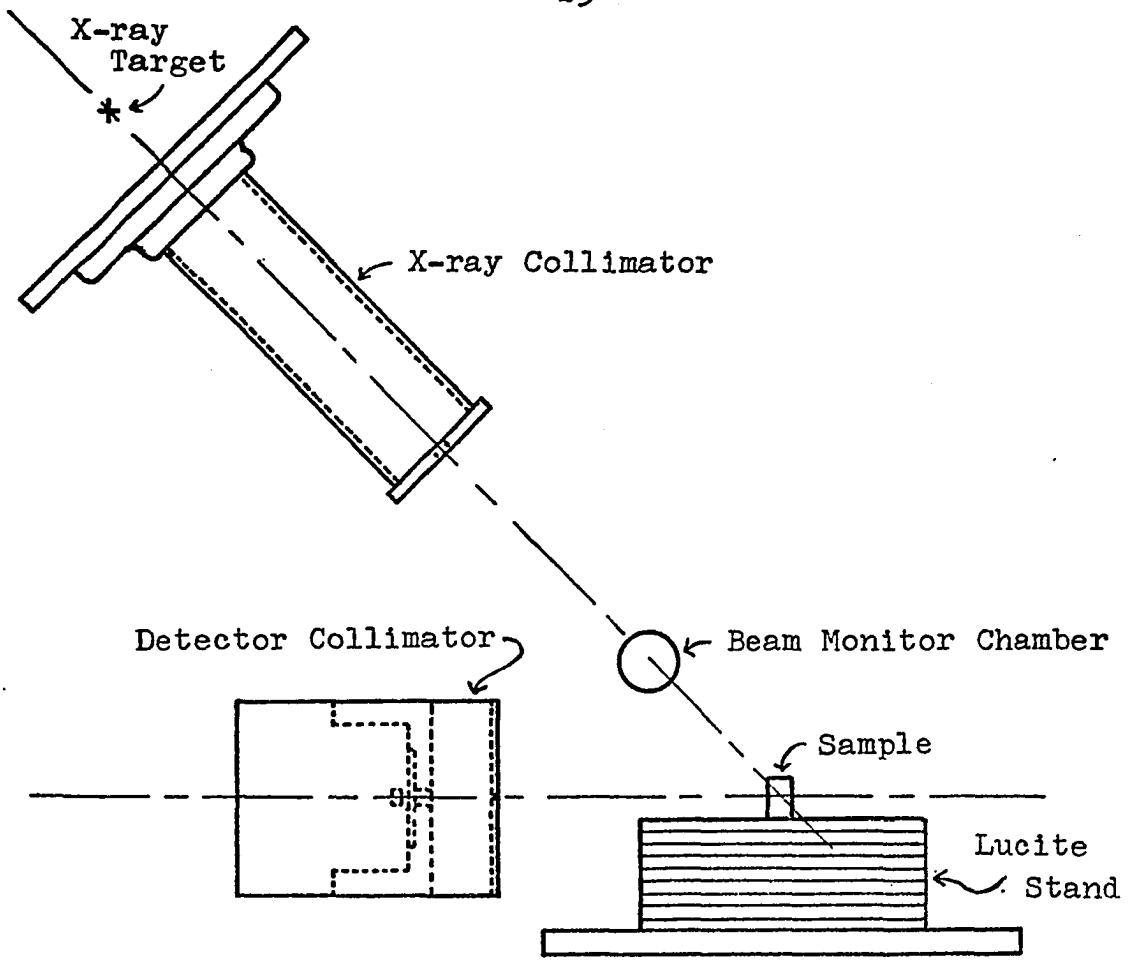

Figure 2-2. Experimental arrangement for measuring sample fluorescence.

Detector

The detector was an Ortec model 8113-0626 high resolution lithium drifted germanium detector. The crystal is planar and has a cylindrical sensitive volume 6 mm. in diameter and 4.92 mm. in depth. The cross section of the active area is 30 square millimeters. It is supported on a right angle cryostat with a 0.13 mm. (5mil) thick beryllium entrance window. The crystal is mounted centrally to and 5 mm. behind the window. The intrinsic efficiency of the crystal to photons as a

function of their energy is shown in Figure 2-3. The detector also has a cooled FET input preamplifier mounted on the cryostat.

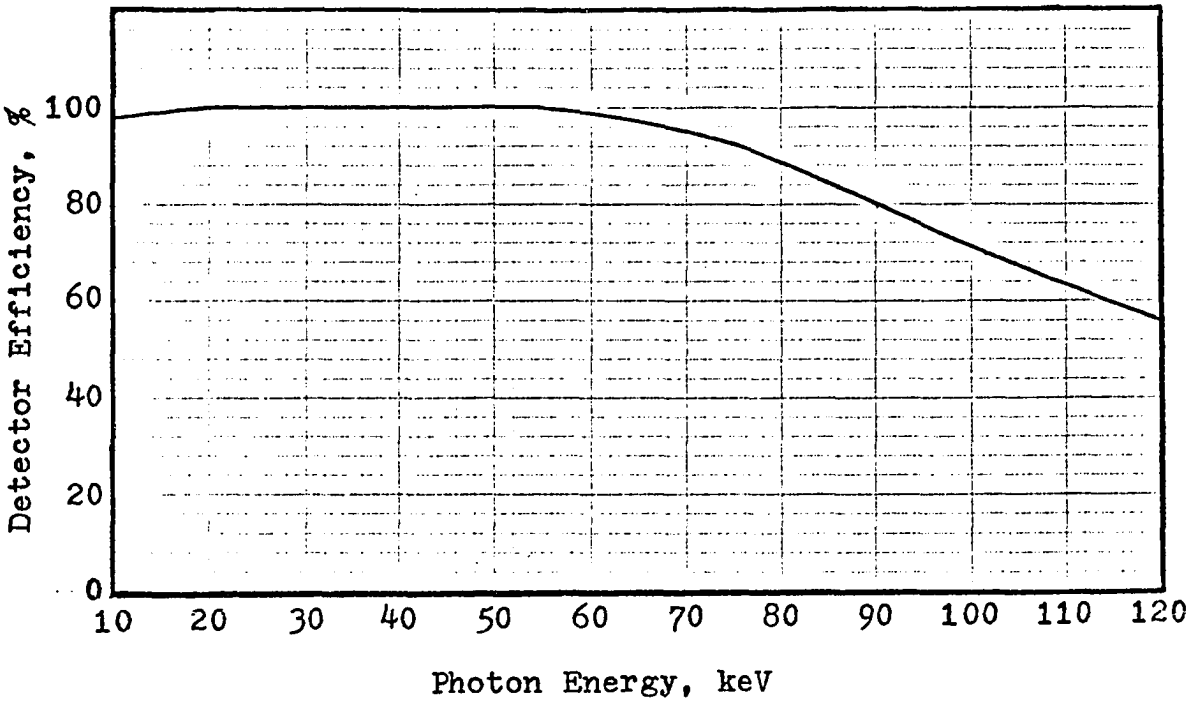

Figure 2-3. Efficiency of Ortec Ge(Li) high resolution spectroscopy crystal (Ortec, 1968).

The detector acceptance solid angle was determined by a double collimator arrangement. This arrangement also served as shielding for the detector as shown in Figure 2-4. The detector acceptance angle could be changed by adjusting the hole size in the interchangeable collimator.

Experimental Assembly

Figure 2-2 shows the experimental arrangement used to measure the fluorescent X-ray fluence from the

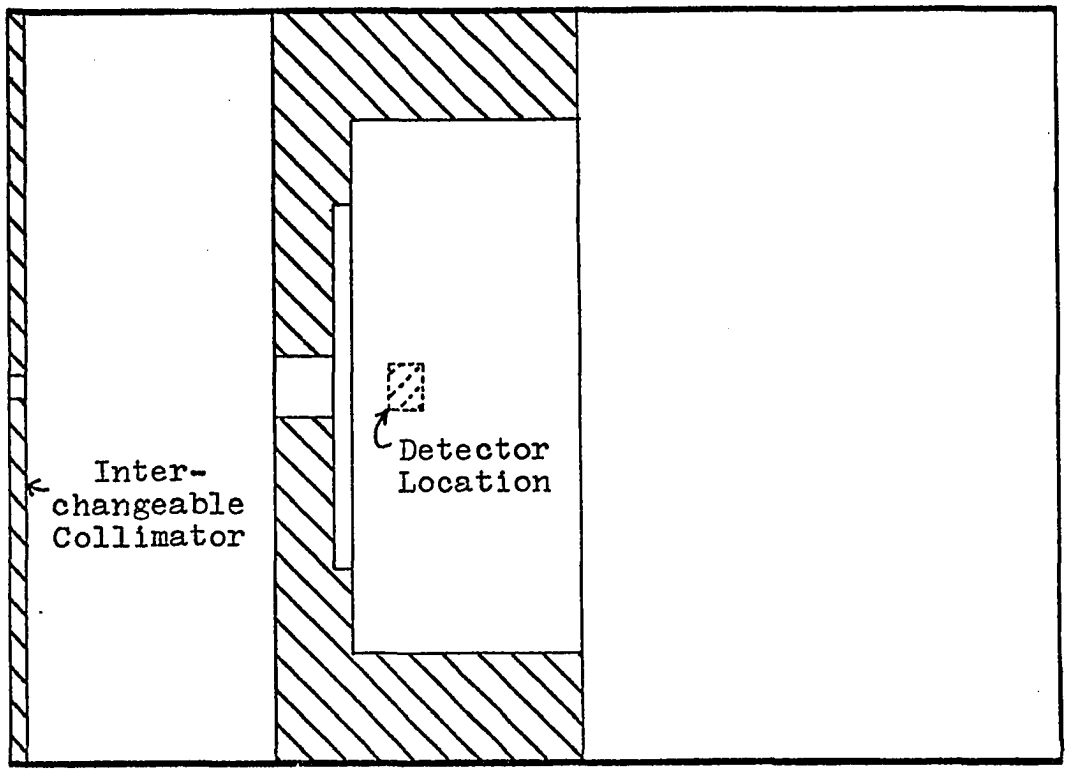

Figure 2-4. Collimator-shield arrangement for the detector. The position of the detector when the collimator is in plane is shown. The outer collimator (left side) is interchangeable.

sample. The X-ray generator was inclined at a 45 degree angle in the vertical plane which also included the sample and the detector. Spatial arrangements for the X-ray generator collimator assembly dictated a minimum target to sample distance of 50 cm. The Victoreen 1 R (model 227) chamber was mounted in the incident beam between the X-ray generator and the sample.

A device for aligning the sample and X-ray generator was constructed by mounting a stainless steel rod along the axis of an empty sample container.

Photographic film was placed under the sample position, the alignment device was placed in the sample position, and the X-ray generator was activated. After irridation the processed film showed the spatial relationship between sample position and incident X-ray beam.

The detector was positioned horizontal with the center of the sample. The detector and sample were aligned visually by shining a light beam through the collimator assembly and observing it on the detector entrance window. When the detector collimator acceptance angle was adjusted so that the entire sample was seen by the detector, the effective cross-sectional area of the detector was 0.079 cm^2 at a sample collimator distance of 15 cm.

A block diagram of the data collecting system is shown in Figure 2-5. The amplifier was an Ortec model 485 active filter amplifier. An Ortec model 408 biased amplifier and Ortec model 411 pulse stretcher were used to select the range of energy presented to the TMC Gammascope 100 channel analyzer. The analyzer was adjusted to the approximate energy range of 60 to 85 keV. This gave the conversion gain of 0.25 keV/channel. The analyzer was calibrated by placing metallic mercury in the sample position and using the mercury fluorescent peaks as the known photon energies.

The value of the ionization current in the ionization chamber mounted in the incident beam was used

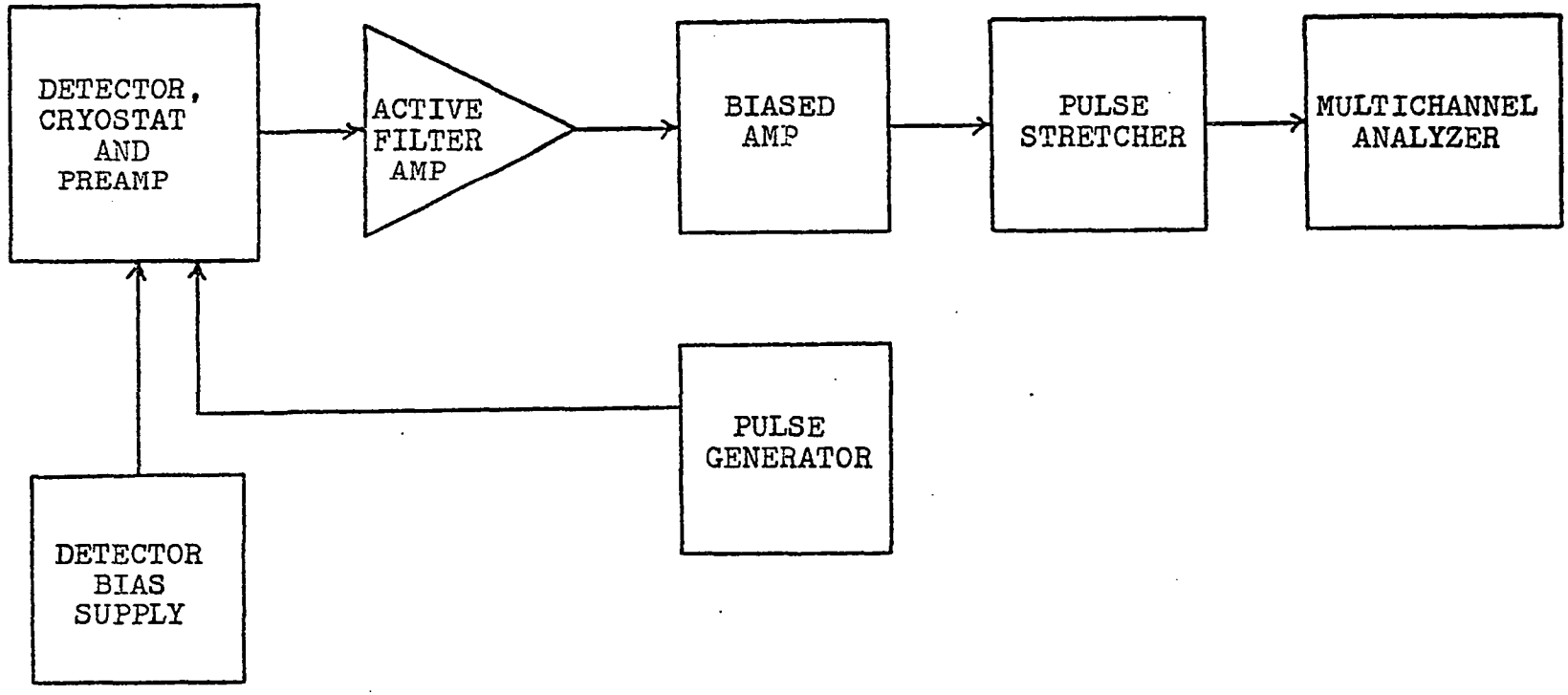

Figure 2-5. Signal path used for X-ray fluorescence measurements.

to monitor the exposure rate in the incident beam. The mA adjustment on the X-ray generator was adjusted as necessary to maintain a constant predetermined exposure rate in the beam.

Incident Fluence Distribution

The energy distribution of fluence of the X-ray beam incident on the sample was measured by aligning the X-ray generator and detector so that the X-ray beam shined on the detector. A collimator with a 0.040 inch diameter hole was used in the outer position on the detector collimator assembly. This was located 140 cm. from the X-ray tube target.

An arrangement consisting of two crossed strings was constructed perpendicular to the X-ray beam in order to define an area of space. This coordinate system was constructed at a distance of 132 cm. from the target. By affixing photographic film to the string and activating the X-ray generator, the coordinate relationship between the strings and X-ray beam was determined.

By knowing both the location of the target and the position of the beam in the plane of the string, the detector and its collimator assembly could be positioned so that the beam shined through this assembly and onto the active area of the detector. The alignment was verified by activating the generator and varying the detector position slightly in all directions. The

alignment that gave the highest attainable count rate was used as the final geometry.

A block diagram of the data collecing system used to measure the incident fluence distribution is shown in Figure 2-6. The pulse generator was used for coarse calibration and checking the overall stability and performance of the system. The amplifier was a Tennelec model 202 BLR with active filter and base line restoration. The amplifier integral and differential time constants were set at 0.8 microseconds. The amplifier output was DC coupled to the ADC of a Kicksort model 711 A multichannel analyzer and also to a single channel analyzer. The lower level discriminator of this single channel analyzer was connected to a scaler for determination of gross count rate.

A subset of 1024 channels was calibrated to approximately 0.2 keV/channel by using the radionuclides Americium-241 and Cobalt-57. Energy determinations on the final measured X-ray spectra were referred to the known energies of the characteristic X-rays from the tungsten X-ray tube target.

Incident Exposure Rate

The exposure rate in the incident beam was measured by placing the 10 R Victoreen chamber in the beam. The chamber was placed at a distance of 125 cm. from the X-ray tube target. The chamber was aligned

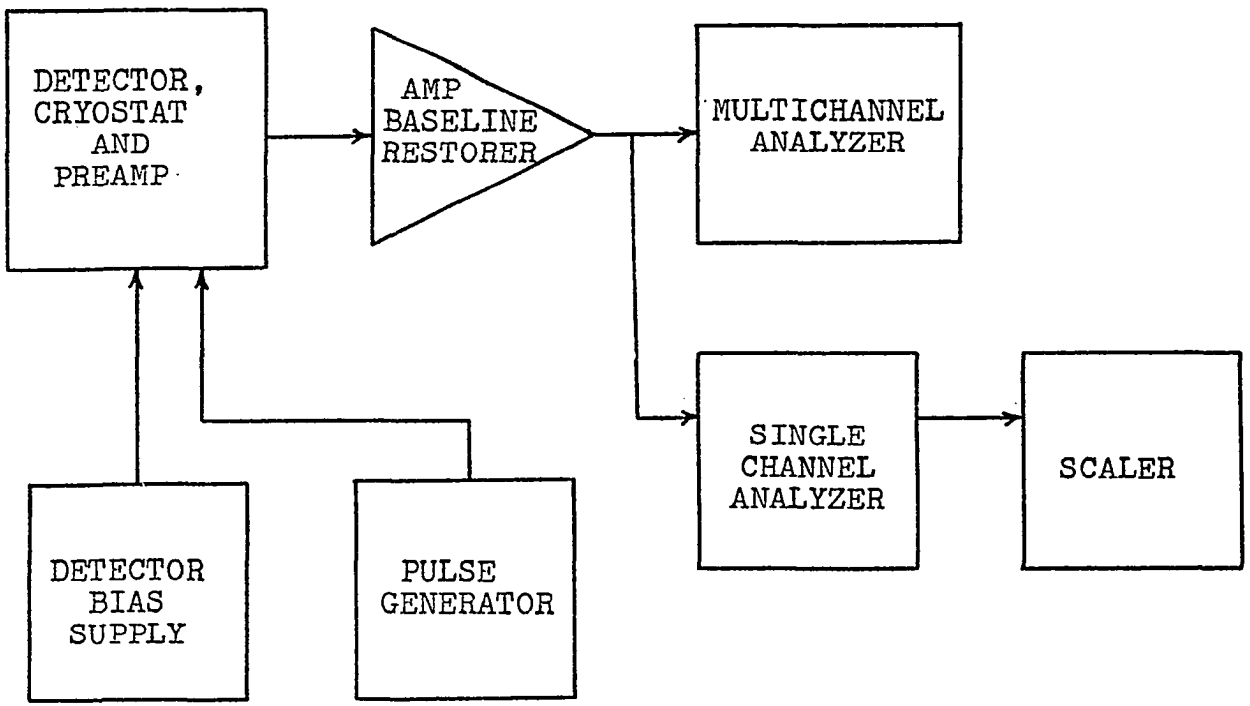

Figure 2-6. Signal path used for measurement of incident beam spectrum.

in the beam by again using the string arrangement described earlier. Photographic film was placed behind the chamber and the resulting radiograph of the chamber assured that the entire chamber was exposed to the beam.

CHAPTER III

EXPERIMENTAL RESULTS

Incident Beam

Beam Attenuation

As the incident beam passes through air away from the X-ray target, two types of attenuation act to reduce the photon fluence. The first and less important of these is air attenuation. This was calculated to be less than two percent for the experimental arrangements; therefore, this error was considered small enough to be neglected in the current investigation.

The second attenuation process is beam divergence. As is well known, this follows an inverse square relationship for a point source of photons. Since the dimensions in the experiment are large in comparison with the X-ray target size, one would expect the inverse square relationship to hold in this case. LiF thermoluminescent dosimeters were used to confirm this expectation by constructing a second string coordinate system similar to the one previously described. The second coordinate system was constructed at a distance of 50 cm. from the X-ray target. The beam position in each string coordinate system was located by using photographic film.

Three groups of six each of 1 mm. x 1 mm. x 6 mm. dosimeters were used to measure the beam attenuation by loading two groups into a 6 mm. x 6 mm. square configuration for exposure. The two groups were affixed to the strings so that they were in the central part of the X-ray beam at the respective distances. These dosimeters were exposed and read out using the third group as a background. The measurement was repeated with the positions of the two exposed groups reversed. The results of the measurements are shown in Table 3-1. The total exposures were of necessity low and consequently the statistical error was large. It was concluded, however, that there was no departure from the expected inverse square relationship.

TABLE 3-1

X-RAY BEAM ATTENUATION

Method	Attenuation Factor	Standard Error
Calculated	6.97	
Run Number 1	6.24	24%
Run Number 2	7.79	25%

Exposure Rate

As described in the previous chapter, the exposure rate in the incident beam was measured with a Victoreen 10R (model 326) ionization chamber. The results of two measurements made at 5 mA for 60 minutes gave an exposure rate of 8.3 mR/mA-min at the sample distance (50 cm.).

Flux Density Spectrum

The energy spectrum was measured using the second experimental arrangement described in the previous chapter. The data were used to determine the X-ray flux density spectrum in the incident beam. The spectrum for a tube potential of 100 kVp is shown in Figure 3-1. This figure was derived from the multichannel analyzer data by, first, correcting for the cross sectional area of the detector collimator, second, correcting for the absolute efficiency of the detector (Figure 2-2), and third, dividing by the product of milliAmps of tube current and the analyzer live time in seconds. A sample of the calculations used in obtaining Figure 3-1 is shown in Appendix A.

Table 3-2 gives the flux density incident on the sample (50 cm.) in the energy range effective in exciting K shell fluorescence in mercury. Appendix A also contains the calculations of these data from the measurement of the incident energy distribution of flux density.

As can be seen in Figure 3-1, the spectrum does not fall to a small value at low energy. This unexpected result is of no concern unless the phenomenon causing it also affects the results at higher energy. To confirm that this was not some form of electrical or magnetic interaction between the X-ray generator and the electronics which might affect the spectrum at higher energy, the beam port of the X-ray generator was sealed off with

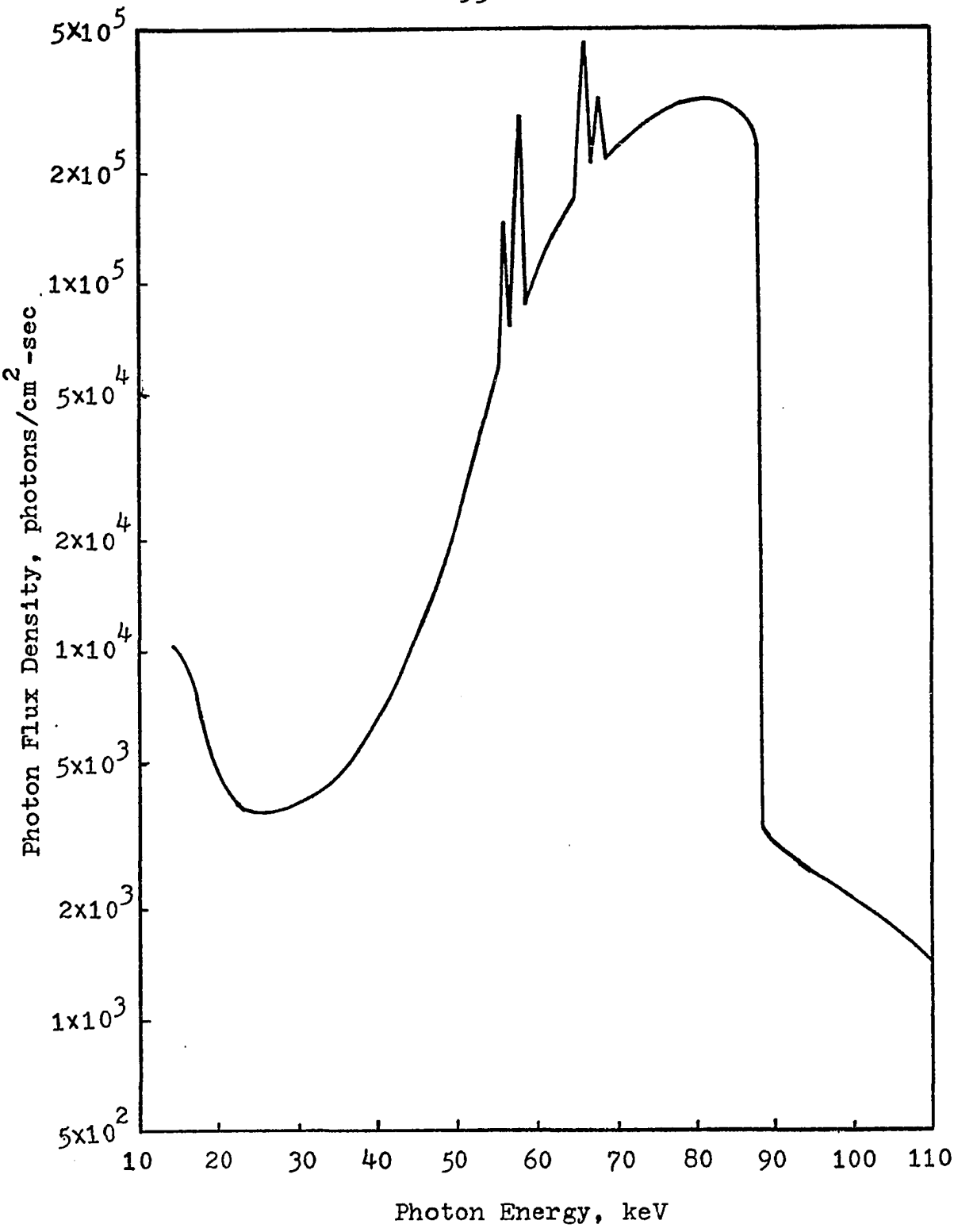

Figure 3-1. X-ray flux density in the incident beam at a distance of 50 cm. from the tube target.

TABLE 3-2

INCIDENT BEAM PHOTON FLUX DENSITY

ΔE (keV)	$\varphi(\Delta E)$ photons/cm^2-sec/mA
83.1 - 84	1.9×10^5
84 - 85	2.1×10^5
85 - 86	2.0×10^5
86 - 87	1.9×10^5
87 - 88	1.8×10^5
88 - 89	3.5×10^4

lead. The X-ray generator and the electronics were operated simultaneously under a variety of conditions. Several spectra were accumulated and cross compared in the analyzer memory. All accumulated spectra consisted of random counts that could be attributed to no other cause than background. The conclusion was that the electronics was unaffected by the X-ray generator.

Although this increase in observed counts in the low energy portion of the spectrum did not affect the experimental calculations, the explanation of this curious effect was pursued further. First, a 0.5 mm. aluminum filter was placed directly against the beryllium window of the detector to determine if the increase in counts was actually due to low energy photons incident on the detector. The filter did not alter the shape of the spectra. It was concluded, therefore, that this increase

was not due to low energy photons entering the detector. Second, the port in the detector collimator was blocked in order to evaluate the detector shielding. A spectrum was obtained with the generator activated and the tube housing port open. This spectrum appeared to be a bremsstrahlung distribution that had been very heavily filtered through lead. The photon flux density in this spectrum was smaller than the flux density in the incident beam by a factor greater than one hundred. No correction was made for this background.

Sample Fluorescence

Emissions

The K shell principal emission lines of mercury and their relative intensities are shown in Table 3-3.

TABLE 3-3

MERCURY K EMISSION LINES

Line	Energy	Relative Intensity
$K\alpha_2$	68.895	50
$K\alpha_1$	70.819	100
$K\beta_3$	79.822	20
$K\beta_1$	80.253	
$K\beta_2^{II}$	82.43	5
$K\beta_2^{I}$	82.54	

It will be noted that the energy difference between $K\beta_3$ and $K\beta_1$ emission lines is 431 eV. As shown in Figure 3-2,

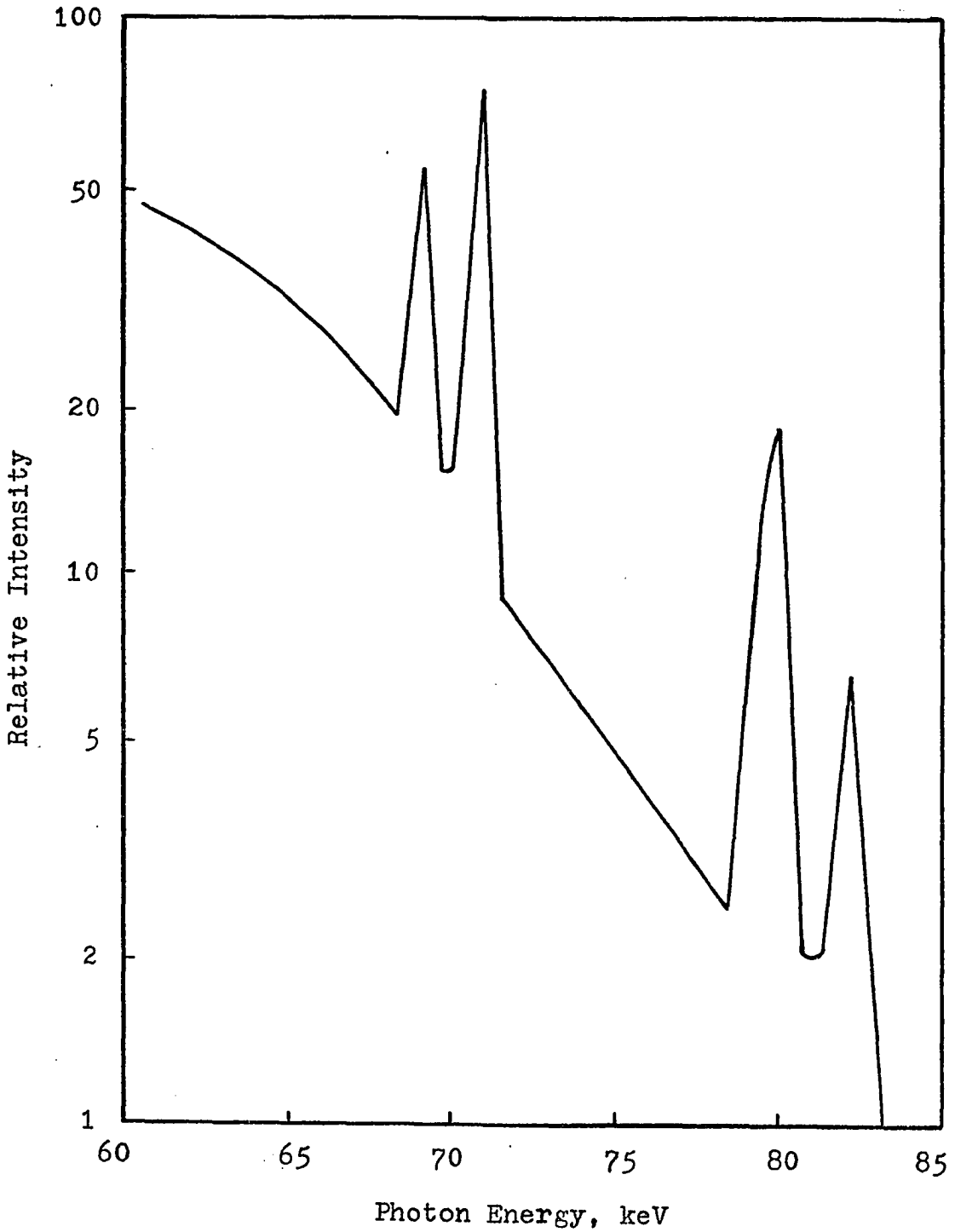

Figure 3-2. Fluorescent peaks from metallic mercury.

the resolution of the detection system is not adequate to separate these two lines. This pair of lines was therefore treated as a single peak in the analysis of the data. The $K\beta_2^{II}$ and $K\beta_2^{I}$ lines are likewise not resolvable. This pair was not used in the data analysis however.

Detectability

The detector fluence from the samples was investigated as a function of the X-ray tube potential used to excite the sample, the mercury concentration in the sample, and the information obtained from each fluorescent line. The measurements were all normalized to an incident total exposure of 25 mR.

In order to determine the optimum X-ray tube potential, constant exposure runs were made at 100, 110, 120, and 130 kVp. The sample for these measurements was the 5637 ppm. mercury solution. The count rates in the two peaks were determined by extending the Compton scatter background under the peaks and summing the differences between channel counts and background. The data and results are shown in Table 3-4.

The total counts that were attributed to the several fluorescent peaks were obtained by making two runs. Each run consisted of the following measurements: water, stock solution, water, dilution one, water, dilution two, water, dilution three, and water. The data

TABLE 3-4

PERCENT STANDARD ERROR FOR EACH TUBE POTENTIAL

Counts and Standard Error	Tube Potential, kVp			
	100	110	120	130
$K\alpha_1$ C.	312	579	512	478
$K\alpha_1$ % S. E.	12.7	8.86	13.4	17.0
$K\beta_1 - K\beta_3$ C.	84.5	137.1	132	128
$K\beta_1 - K\beta_3$ % S. E.	17.0	15.3	20.1	79.1

from the concentration measurements appears in Appendix B. This data was used to calculate the detectability of the $K\alpha_1$ and the $K\beta_1 - K\beta_3$ peaks by first summing the peak area for each observation. The channels used for the $K\alpha_1$ peak were 39 through 45 and for the $K\beta_1 - K\beta_3$ peak were 75 through 80. The peak areas for the water sample in each run were averaged and this average subtracted from the mercury samples in each run. Tables 3-5 and 3-6 give the results of these calculations.

TABLE 3-5

CONCENTRATION RESULTS FOR $K\alpha_1$ PEAK

Concentration	First Run	Second Run
5637	293	309
3780	201	237
2835	153	190
1890	146	69

TABLE 3-6

CONCENTRATION RESULTS FOR $K\beta_1$ - $K\beta_3$ PEAK

Concentration	First Run	Second Run
5637	81.3	79.4
3780	42.3	44.4
2835	49.3	26.4
1890	12.3	25.4

The average of the $K\alpha_1$ results is shown in Figure 3-3 and the average of the $K\beta_1$ - $K\beta_3$ results is shown in Figure 3-4.

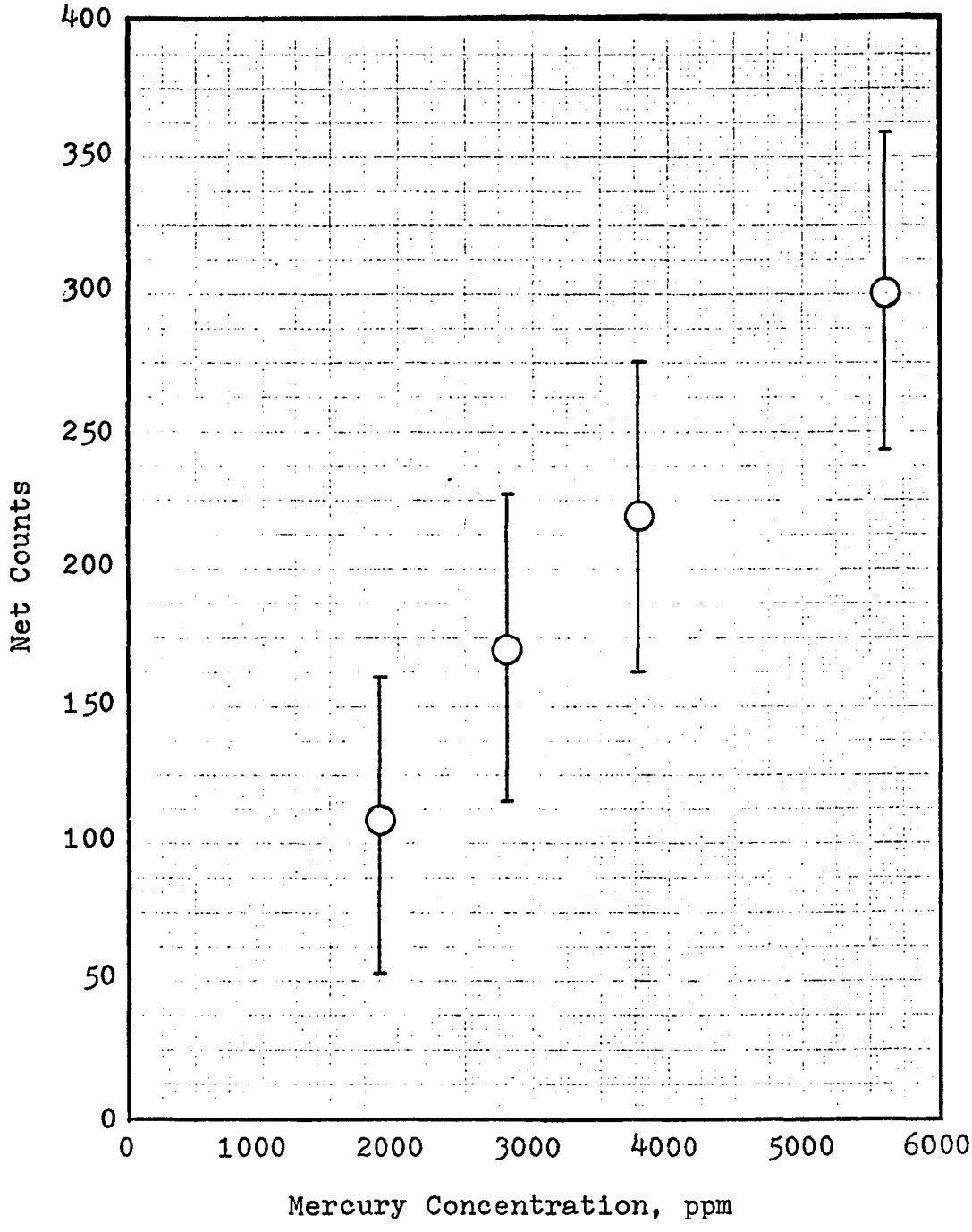

Figure 3-3. Net counts as a function of concentration for $K\alpha_1$ peak.

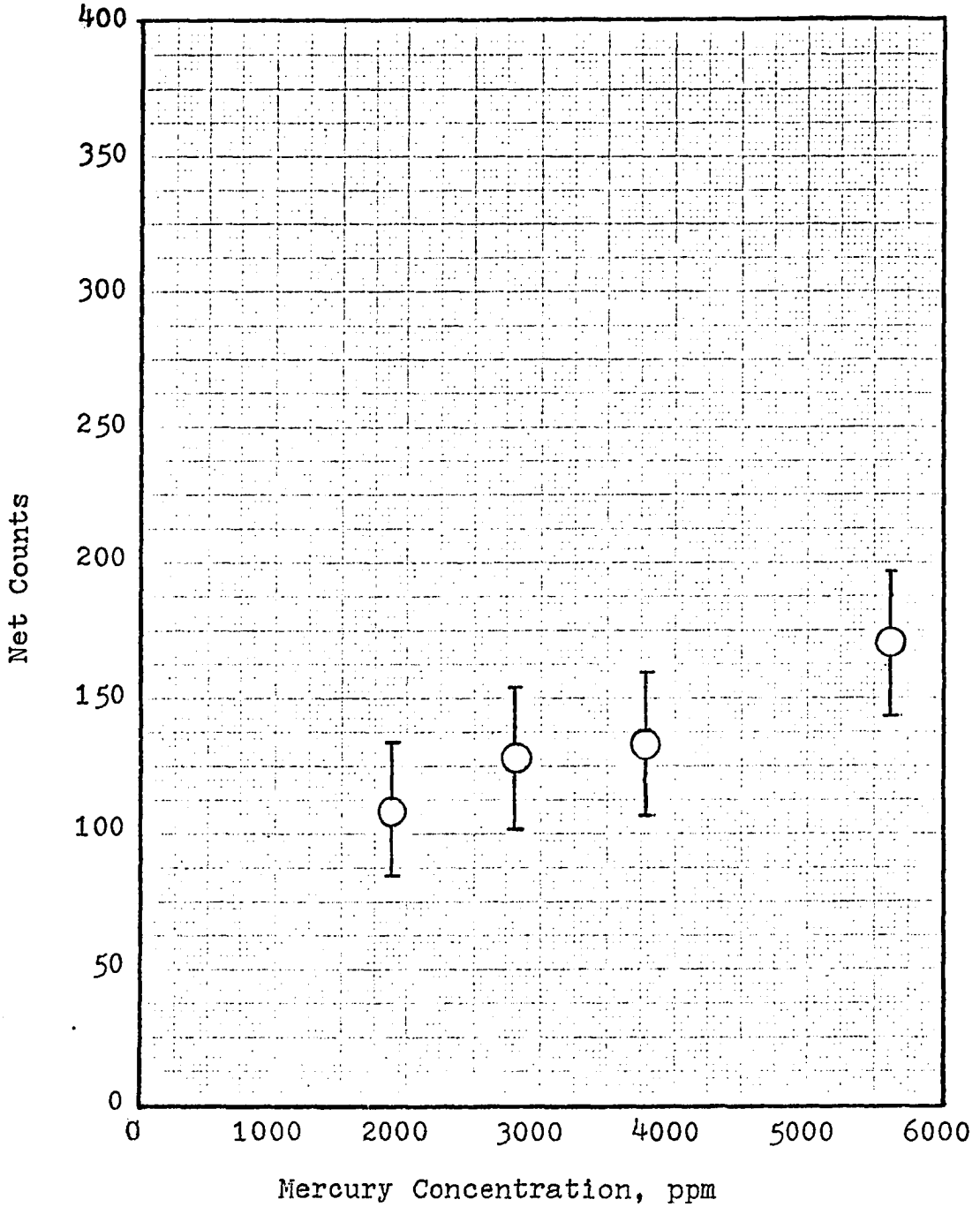

Figure 3-4. Net counts as a function of concentration for $K\beta_1$ - $K\beta_3$ combination peak.

CHAPTER IV

DISCUSSION AND CONCLUSION

The lower range of detectability of mercury with an X-ray generator may be estimated by examination of Figures 3-3 and 3-4. The point at which the net counts approaches the standard error is in the order of 1000 ppm; a value several orders of magnitude too large for in vivo use. The figures do suggest, however, that the relative standard error is nearly independent of mercury concentration. Table 4-1 gives the mercury concentrations and the relative standard errors for the $K\alpha_1$ and $K\beta_1$ - $K\beta_3$ peaks. These data substantiate the observation that

TABLE 4-1

RELATIVE STANDARD ERRORS

Dilution	$K\alpha_1$	$K\beta_1$ - $K\beta_3$
5637	58	27
3780	56	26
2835	55	25
1890	54	25

the relative standard errors are nearly independent of concentration. This important result is explained by the fact that for excitation with an X-ray generator, the Compton background contribution at the measured

energies is much greater than the sample fluorescence contribution at the same energies. This result also places severe limits on the usefulness of the X-ray generator at low concentrations.

The concentration data were used in the following way to confirm the results of the discussion in the first chapter. For the current experiment the attenuation of the incident and fluorescent X-rays by the sample is negligable. Equation (1-2) for this case reduces to

$$\Delta \Phi_{D,E_L} = \frac{S\Delta t}{4\pi R^2} C_A \left(\frac{r_n - 1}{r_n}\right) \omega_n g_L \times \int_{E_n}^{E_{max}} [\mu/\rho]_A(E_o) \Phi_{in}(E_o) dE_o \quad . \tag{4-1}$$

For the $K\alpha_1$ line and the current experimental arrangement the constants are as follows:

$$S\Delta t = 2.5 \text{ cm}^3$$
$$R = 50 \text{ cm}$$
$$C_A = 5.6 \times 10^{-3} \text{ gm/cm}^3 \text{ (5600 ppm)}$$
$$g_{K\alpha_1} = 100/175$$
$$r_n = 4.8$$
$$\omega_n = 0.95$$

The integral was evaluated by summing the products of the fluences in Table 3-2 and the mass absorption coefficients at each energy. The value of the partial

fluence at the detector from the $K\alpha_1$ line, $\Phi_{D,K\alpha_1}$, was found to be 16.3 photons per cm^2 per mAs. Correcting for the detector efficiency and the detector area gives a net count of 1.36 counts per mAs. Since the exposure rate was measured to be 8.3 mR per mAmin, the total number of counts is 244. This value compares favorably with the 301 counts shown in Figure 3-3.

The results that would have been obtained by substituting a radionuclide source for the X-ray generator can be predicted by examining the physical process. The Compton scatter contribution in the two cases is markedly different. For the case of excitation with an energy distribution of photons, the Compton background is continuous through the fluorescent peak area. However, in the case of discrete energy excitation, the Compton scatter appears at the detector at nearly discrete energies that are given by equation (1-5). If this discrete energy can be selected so that the Compton scatter does not fall in or near the fluorescent peak, the background is very small. Under this condition the standard error is almost entirely due to the sample counts and is given as the square root of the sample count. Clearly this is a function of the mercury concentration and decreases as the sample concentration decreases.

A radionuclide source that is best suited to the excitation of mercury has the following properties: gamma emission energy greater than the mercury K absorption

edge energy, gamma emission of high absolute intensity, long half-life, readily available in large quantity, and easy to handle. The search for such a radionuclide was largely unrewarding. For the purpose of comparison, however, the radionuclide Cobalt-57 was chosen for the calculation. This isotope has a half-life of 270 days and emits two gamma rays with energies 122 keV (87%) and 136 keV (11%). The calculation was made as if the radioactive source were positioned exactly as the X-ray target so that the results would be directly comparable with those obtained with the X-ray generator. The value of the partial fluence at the detector form the $K\alpha_1$ line was calculated from the equation

$$\Delta\Phi_{D,E_{K\alpha_1}} = \frac{S\Delta t}{4\pi R^2} C_A \left(\frac{r_n - 1}{r_n}\right) \omega_n g_{K\alpha_1} \sum^{E_o} [\mu/\rho]_{A,E_o} \Phi_{in,E_o} \tag{4-2}$$

and found to be 2.4 photons per cm^2 per Ci-sec. Using a value of 90 mR per hr-Ci at one meter for the specific γ-ray constant, the total number of counts is found to be 47.4 counts for a 25 mR exposure. The standard error associated with this value (15%) is approximately equal to that obtained with the X-ray generator with background subtraction (13%). This factor of two combined with the fact that the Cobalt-57 gamma rays are far from the optimum energy and the experimental arrangement is not optimum for radionuclide excitation suggests that the

lower detection limit for aqueous mercury has not been approached.

The experimental results show that the use of an X-ray generator to excite X-ray fluorescence from in vivo mercury is of no practical use. The situation is more promising with a radionuclide as the source of excitation although the minimum detectable concentration currently obtainable is much too high to be of practical significance. This condition may change, however, with optimization of experimental parameters together with improvements in the hardware used in this type of measurement. Improvements in pharmaceuticals tagged with stable mercury also may help make this element practical for in vivo diagnostic studies.

BIBLIOGRAPHY

Bearden, J. A. (1967). X-ray wavelengths and X-ray atomic energy levels. Natl. Bur. Std. (U. S.), NSRDS-NBS 14.

Bertin, Eugene P. (1970). "Principles and Practice of X-Ray Spectrometric Analysis." Plenum Press, New York.

Cameron, J. F., and Rhodes, J. R. (1963). Filters for energy selection in radioisotope X-ray techniques. In "Encyclopedia of X-Rays and Gamma Rays" (G. L. Clark, ed.), p. 387-392. Reinhold, New York.

Clark, George L. (1955). "Applied X-rays." 4th ed. McGraw-Hill, New York.

Compton, Arthur H., and Allison, Samuel K. (1935). "X-Rays in Theory and Experiment." D. Van Nostrand, New York.

Evans, Robley D. (1955). "The Atomic Nucleus." McGraw-Hill, New York.

Evans, Robley D. (1968). X-ray and γ-ray Interaction. In "Radiation Dosimetry" 2nd ed. Academic Press, New York.

Hoffer, Paul B., Jones, W. Barclay, Crawford, Richard B., Beck, Robert, and Gottschalk, Alexander. (1968). Fluorescent Thyroid Scanning: A New Method of Imaging the Thyroid. Radiology 90, 342-344.

Hoffer, Paul B. (1969a). Fluorescent Thyroid Scanning. American Journal of Roentgenology 105, 721-727.

Hoffer, Paul B., Polcyn, Robert E., Moody, Robert, Lowe, Henry J., Gottschalk, Alexander. (1969b). Fluorescence Detection: Application to the Study of Cerebral Blood Flow. Journal of Nuclear Medicine 10, 651-653.

Hoffer, Paul B., Beck, Robert N., Lembares, Nicholas, Charleston, Donald B., and Gottschalk, Alexander. (1971). Use of Lithium Drifted Germanium Detectors for Clinical Radionuclide Scanning. Journal of Nuclear Medicine 12, 25-27.

Hubbell, J. H. (1969). Photon cross sections, attenuation coefficients, and energy absorption coefficients from 10 keV to 100 GeV. Natl. Bur. Std. (U. S.), NSRDS-NBS 29.

Klein, O., and Nishina, Y. (1929). Zeit Fur Physik 52, 853.

Morgan, K. Z., and Turner, J. E. (1967). "Principles of Radiation Protection." John Wiley and Sons, New York.

ORTEC. (1968). Instruction manual semiconductor X-ray spectrometer system.

Patton, James A., Erickson, Jon J., and Brill, A. B. (1970). Study of the Feasibility of Bismuth Fluorescence Scanning Using a Cylindrical Array Tomographic Scanner. Journal of Nuclear Medicine 11, 346.

Robin, G., Broquet, C., and Vacher, M. (1967). Realisation and use of X-ray filters for energy selection. In "Proceeding of 2nd Symposium of Low-Energy X- and Gamma Sources and Applications" (P. S. Baker et al., eds), p. 356-375. USAEC, ORNL-11C-10 (Vol. 1).

Tinney, J. F. (1967). High-Z Element Fluorescent X-rays For In Vivo Biological Studies. Ph. D. Dissertation, University of Oklahoma.

APPENDIX A

SAMPLE OF INCIDENT BEAM FLUX DENSITY CALCULATION

A partial listing of the analyzer data from the energy spectrum measurement is reproduced below.

Channel			
400-410	411-421	422-432	433-443
2853	2793	2618	542
2849	2770	2572	183
2814	2800	2539	59
2866	2717	2540	27
2817	2783	2387	41
2878	2580	2417	30
2844	2780	2348	19
2838	2718	2239	26
2854	2704	2013	20
2708	2599	1594	25
2714	2600	1002	19

As previously discussed the characteristic X-rays from the tungsten target were used for the final energy calibration. The calibration equation is

$$N = \frac{E - 6}{0.19}$$

where N = channel number

and E = photon energy in keV .

The equation was used to assign channels to each energy increment. The channel assignments are as follows:

Energy Increment (keV)	Channel
82 - 83	400 - 405.3
83 - 84	405.3 - 410.5
84 - 85	410.5 - 415.8
85 - 86	415.8 - 421.1
86 - 87	421.1 - 426.3
87 - 88	426.3 - 431.6
88 - 89	431.6 - 436.8
89 - 90	436.8 - 442.1

The photon flux density per milliAmp per keV at a distance of 140 cm. was determined by summing the counts in each channel or fraction of a channel and assigning this sum to each energy increment. These assignments were as follows:

Energy Increment							
82-83	83-84	84-85	85-86	86-87	87-88	88-89	89-90
2853	2015	1357	557	2340	1671	638	5
2849	2844	2793	2580	2618	2417	1002	41
2814	2838	2770	2780	2572	2348	542	30
2866	2854	2800	2718	2539	2239	183	19
2871	2708	2717	2704	2540	2013	59	26
863	1357	2226	2599	716	953	22	20
			260				3

These sums were divided by the absolute efficiency of the detector (Figure 3-2), the area of the beam passed by the detector collimator (8.11×10^{-3} $cm.^2$), and the product of the beam current and analyzer live time (79.96 mAs). This flux density at 140 cm. was converted to the flux density at 50 cm. by the inverse square relation (7.84). These results are summarized below.

E(keV)	Sum	φ @ 140 cm.	φ @ 50 cm.
82 - 83	15116	2.78×10^4	2.18×10^5
83 - 84	14616	2.69×10^4	2.11×10^5
84 - 85	14663	2.69×10^4	2.11×10^5
85 - 86	14198	2.60×10^4	2.04×10^5
86 - 87	13325	2.45×10^4	1.92×10^5
87 - 88	11644	2.25×10^4	1.76×10^5
88 - 89	2446	4.41×10^3	3.46×10^4
89 - 90	144	2.77×10^2	2.17×10^3

Figure 3-1 was plotted from the complete set of data while Table 3-2 was taken from this subset of data.

APPENDIX B

ANALYZER DATA FROM CONCENTRATION MEASUREMENT

FIRST RUN

WATER 1

Channel

1-25	26-50	51-75	76-99
689	393	53	10
700	348	40	15
1140	274	36	14
1056	253	43	14
1049	205	31	9
1028	192	40	19
1023	166	37	17
994	151	36	10
1012	141	46	14
970	135	26	14
917	109	24	13
980	93	28	11
908	114	40	10
892	108	28	9
864	88	12	11
846	80	16	7
803	72	24	9
754	69	18	7
763	64	18	8
696	51	16	7
623	59	10	12
619	47	14	2327
563	53	24	14475
545	51	14	1920
481	44	11	

FIRST RUN

WATER 2

Channel

1-25	26-50	51-75	76-99
740	485	49	22
699	381	56	22
1218	340	42	10
1141	326	24	9
1131	225	37	7
1175	189	33	18
1092	199	30	16
1039	181	41	11
1080	151	38	17
1093	161	35	11
1033	129	31	11
1072	121	35	11
1008	120	29	17
981	96	27	12
1046	98	24	8
900	99	14	8
915	86	26	11
842	81	24	10
785	63	27	8
733	76	19	9
746	71	15	12
730	74	17	2187
623	58	16	14613
625	57	21	1962
517	53	16	

FIRST RUN

WATER 4

Channel

1-25	26-50	51-75	76-99
707	431	52	11
592	351	44	22
1108	336	38	14
1083	266	40	16
1049	241	34	11
1099	225	36	13
974	186	34	16
1071	157	24	13
1026	150	32	10
981	163	33	12
943	127	31	6
966	107	21	10
946	119	22	10
935	81	30	9
891	76	16	9
867	91	23	9
887	80	15	12
814	75	16	13
783	66	24	5
680	66	19	12
654	71	17	12
632	82	16	1978
627	55	19	14491
556	66	13	2274
507	40	17	

FIRST RUN

WATER 5

Channel

1-25	26-50	51-75	76-99
721	423	52	12
599	389	47	21
1116	322	44	7
1046	266	46	13
1011	208	36	12
1036	214	40	9
932	166	34	9
939	181	31	12
1008	152	31	9
994	135	25	9
946	116	29	16
970	92	25	8
898	112	18	15
914	95	18	12
880	84	28	7
852	83	23	10
825	73	27	14
812	79	16	6
671	67	16	8
723	61	20	6
615	64	16	12
646	57	20	2057
567	44	18	14567
554	42	9	2112
500	56	16	

FIRST RUN

Hg SOLUTION

Channel

1-25	26-50	51-75	76-99
743	445	45	16
749	396	38	35
1135	338	46	39
1113	269	46	38
1099	247	53	17
1124	223	45	16
1053	232	33	12
987	179	43	19
998	179	34	13
1023	187	38	10
1032	166	37	16
962	132	30	13
989	127	30	14
933	106	27	16
907	93	19	8
929	154	20	15
837	162	16	7
827	170	22	12
789	91	21	14
792	69	25	12
746	76	30	13
680	61	15	2242
623	59	22	14658
559	78	19	1858
511	52	19	

FIRST RUN

2:1 DILUTION

Channel

1-25	26-50	51-75	76-99
634	433	39	17
638	377	42	23
1090	314	42	30
1065	258	36	24
1052	247	38	14
1039	227	45	15
1061	153	25	12
969	159	43	17
980	174	33	11
967	200	33	13
949	158	21	16
977	96	24	17
889	98	19	12
926	99	27	8
887	108	14	5
877	126	23	15
790	140	18	6
753	146	24	11
763	81	21	16
690	53	17	10
686	64	13	17
614	46	19	2179
619	51	13	14611
566	47	22	1941
497	53	17	

FIRST RUN

1:1 DILUTION

Channel

1-25	26-50	51-75	76-99
701	421	41	13
634	386	39	25
1163	325	40	27
1107	326	37	26
1035	222	42	23
1040	191	30	13
994	181	41	12
944	184	31	12
947	172	28	10
1010	165	37	13
938	132	30	11
991	120	23	13
978	98	24	20
938	100	24	17
892	112	16	17
870	109	19	6
852	135	22	10
773	107	22	6
792	90	14	11
707	52	14	11
690	63	13	11
663	63	19	1933
592	46	18	14585
539	56	14	2223
512	50	18	

FIRST RUN

1:2 DILUTION

Channel

1-25	26-50	51-75	76-99
668	427	35	17
567	371	40	17
1126	327	33	16
1091	260	35	18
1022	228	46	14
1017	193	44	17
965	149	38	15
944	209	32	18
955	181	32	10
992	154	27	7
908	116	27	8
924	120	18	12
881	91	20	14
875	112	14	17
891	114	24	12
882	92	18	11
774	117	17	13
794	94	15	7
696	99	27	11
697	70	16	11
682	60	12	13
605	60	13	2070
590	59	22	14468
555	44	7	2203
493	48	13	

SECOND RUN

WATER 1

Channel

1-25	26-50	51-75	76-99
723	443	44	11
681	355	46	23
1146	356	41	20
1156	260	32	15
1035	253	40	17
1108	205	31	12
1139	191	39	14
1121	167	40	11
1089	149	35	12
1039	153	29	9
1013	140	23	7
1074	109	30	16
1040	141	26	12
1019	103	29	19
971	84	17	6
873	95	26	8
865	77	13	12
801	80	24	13
767	60	22	9
792	79	20	13
709	51	18	10
685	62	17	2023
554	61	24	14592
621	55	16	2114
486	36	10	

SECOND RUN

WATER 2

Channel

1-25	26-50	51-75	76-99
714	424	40	21
651	372	32	21
1103	311	38	11
1115	261	43	15
1049	240	40	14
1003	198	43	15
1022	186	42	9
974	121	34	7
909	143	25	8
936	112	29	13
1001	118	25	9
962	105	28	9
959	123	18	14
966	87	26	9
909	91	21	7
872	72	22	10
814	86	19	13
796	73	22	7
717	53	25	8
743	68	21	11
671	72	23	8
617	48	22	2107
577	54	17	14568
510	53	18	2069
461	51	19	

SECOND RUN

WATER 3

Channel

1-25	26-50	51-75	76-99
699	411	39	15
630	361	37	15
1161	301	46	14
1104	273	43	15
1099	235	38	15
1049	194	26	9
1038	181	28	11
1020	180	36	16
1030	159	29	10
1069	161	35	13
1041	140	24	17
973	106	34	12
944	135	17	11
964	103	31	8
901	90	23	15
874	89	25	17
851	74	22	8
802	78	19	9
735	71	20	7
748	64	16	11
743	78	14	6
637	69	15	2158
618	62	17	14650
566	59	15	1938
499	57	19	

SECOND RUN

WATER 4

Channel

1-25	26-50	51-75	76-99
685	413	38	14
691	337	49	13
1082	299	30	20
1060	268	31	19
1041	227	44	7
1032	158	23	12
1059	180	46	18
1013	157	39	14
955	152	32	13
1024	136	30	11
945	135	23	17
981	120	29	9
973	115	34	6
855	102	26	7
934	81	28	8
846	90	25	10
830	75	16	10
814	69	27	10
782	70	22	12
695	61	28	8
659	59	17	7
633	60	22	2064
578	53	20	14613
496	45	17	2075
488	38	14	

SECOND RUN

WATER 5

Channel

1-25	26-50	51-75	76-99
773	443	39	15
616	378	35	16
1146	355	37	25
1159	288	48	15
1158	242	45	18
1112	185	41	16
1178	196	36	12
1149	186	39	10
1122	175	42	15
1083	130	39	7
1030	139	29	12
1024	131	32	16
1052	129	27	10
966	107	27	14
1001	101	25	9
961	93	29	3
866	80	16	11
875	75	14	8
799	66	15	8
745	70	17	7
689	67	14	6
674	67	11	2039
602	61	18	14603
612	53	16	2101
563	52	17	

SECOND RUN

Hg SOLUTION

Channel

1-25	26-50	51-75	76-99
686	400	35	13
699	342	32	37
1042	322	33	48
1046	260	44	32
1049	219	41	24
1015	167	37	15
1069	177	32	11
1053	168	35	9
1024	159	38	14
979	118	36	7
932	126	26	10
926	119	29	14
954	117	25	9
873	92	24	12
905	93	23	9
870	102	27	3
783	176	14	10
792	182	12	7
723	133	13	7
674	94	15	6
623	61	12	6
610	61	10	2214
544	55	16	14601
554	48	15	1918
510	47	22	

SECOND RUN

2:1 DILUTION

Channel

1-25	26-50	51-75	76-99
701	451	42	24
624	396	34	29
1179	331	40	21
1186	278	46	27
1120	255	42	17
1077	211	45	15
1092	198	44	9
1045	129	36	8
969	152	27	8
997	119	31	14
1062	126	27	10
1024	112	30	9
1020	131	20	15
1027	97	28	9
967	122	23	7
928	134	23	10
867	162	20	13
847	126	23	7
764	71	27	9
790	89	23	11
714	76	25	8
656	52	24	2107
614	58	19	14582
543	57	20	2064
491	55	23	

SECOND RUN

1:1 DILUTION

Channel

1-25	26-50	51-75	76-99
785	422	39	10
623	345	50	26
1118	306	31	31
1099	274	31	32
1076	232	45	8
1062	162	24	13
1084	184	47	18
1045	161	40	15
977	155	33	13
1051	139	30	11
967	137	24	17
1007	123	30	9
995	118	35	6
875	109	27	7
955	97	28	8
866	130	26	11
849	138	17	11
832	106	27	11
799	110	23	12
712	63	28	8
674	60	17	8
648	61	22	2199
591	54	20	14513
508	46	18	2035
499	39	16	

SECOND RUN

1:2 DILUTION

Channel

1-25	26-50	51-75	76-99
723	422	42	13
672	338	43	27
1097	339	39	30
1100	248	29	24
982	241	37	19
1063	195	29	11
1088	181	37	14
1070	159	38	10
1044	141	33	12
998	146	27	9
965	133	22	7
1031	104	28	15
994	104	25	11
971	92	27	18
925	101	16	5
830	99	25	8
823	100	13	12
762	109	23	13
730	67	22	8
756	64	19	13
675	48	18	10
653	59	16	2103
526	59	24	14527
592	52	16	2107
463	34	9	